ISSN 1054-660X, Laser Physics, 2009, Vol. 19, No. 6, pp. 1312–1322.




# Skin Optical Clearing for Improvement of Laser Tattoo Removal[1]

**A. N. Bashkatov[a], *, E. A. Genina[a], V. V. Tuchin[a], and G. B. Altshuler[b]**

[a] *Department of Optics and Biomedical Physics of Saratov State University, Saratov, 410012 Russia*
[b] *Palomar Medical Technologies Inc., 82 Cambridge St., Burlington 01803 MA, USA*
e-mail: a.n.bashkatov@mail.ru
Received November 28, 2008

**Abstract**—The possibility of improvement of laser tattoo removal due to the optical clearing of human skin is investigated. It is shown experimentally that previously perforation of skin stratum corneum allows increasing tattoo image contrast at topical administration of immersion agent in contrast with non-perforated skin. Computer Monte Carlo simulation shows that at the optical clearing of upper skin layers the tattoo image contrast and the photon fraction absorbed in the tattoo area at the depths of 0.5 or 1.0 mm increase, that allows significant decreasing of the power of laser radiation used at laser thermolysis.

PACS numbers: 87.64.Cc; 87.10.Rt; 87.15.Vv; 87.57.cj; 87.85.Pq

**DOI:** 10.1134/S1054660X09060231

## 1. INTRODUCTION

The problem of tattoo removal is as old as tattooing. In many cosmetic clinics the destructive methods of tattoo removal such as dermabrasion and argon or $CO_2$ laser vaporization of upper skin layers are still widely used [1–3], but they have a high risk of scarring. The method of tattoo pigment removal by the use of laser selective thermolysis is effective and safe enough [4–6]. Because of the variety of tattoo ink colors, a variety of laser wavelengths are necessary. Nanosecond (10–100 ns) pulsed lasers of red and NIR spectral regions, such as ruby laser (694 nm) [4–9] and Q-switched lasers, for example Nd:YAG (1064 and 532 nm) [5–9] and alexandrite (700–850 nm) [6, 9–11], are the most often used for the purposes.

Pigmented ink particles used for tattoo are found within dermal fibroblasts and mast cells, predominantly in a perivascular location [12]. Red and NIR laser radiation penetrates deeply enough into skin and it is absorbed strongly by blue, green, and black tattoo pigments included in the composition of the most tattoos [6]. Upon irradiation of skin by short laser pulses the heating and the thermal destruction of pigment particles takes place significantly quicker than the heating of surrounding dermal tissue [9, 10]. The destruction of ink particles and cells containing them, allows organism to remove the pigments by means of normal physiology with the help of lymphatic transport [13, 14].

The number of laser therapy sessions depends on the type of ink, the depth of tattoo location and the laser type. For some tattoos, deep-pigmented layers may be screened by superficial ones, which require multiple laser treatments [10, 15]. An additional difficulty appears because some multicolor tattoos contain pigments, which slightly absorb NIR radiation [14, 16]. Although, shortwave radiation is well absorbed by tattoo pigments, the use of the lasers of visible spectral range is limited by high light scattering in skin and hemoglobin absorption [6]; whereas an increase of intensity of laser radiation for compensation of energy losses related with light scattering and absorption in tissue can produce the tissue damage including a stable pigmentation of skin.

Optical immersion of skin [17, 18] based on the matching of the refractive indices of scattering centers (collagen and elastin fibers) and surrounding matter (interstitial fluid) can be suggested as a promising technique to solution of the problem. Evidently that the immersion will promote the improvement of laser light delivery to the embedded ink particles due to the decrease of light scattering in skin. It will allow the use of the laser radiation of visible spectral range, which in a number of cases can be more effective at the action on the certain types of dyes.

A number of laser surgery and therapy technologies may have a significant benefit at a reversible skin scattering reduction. However, slow diffusion of optical clearing agents (OCAs), such as glucose or glycerol solutions, through human skin barrier makes practical application of optical immersion difficult. To reduce barrier function of skin epidermis a number of different chemical and physical methods such as stripping [19], microdermabrasion [20], laser ablation of skin surface [21, 22], iontophoresis [23, 24], ultrasound [25] and photomechanical waves [26], and needle-free injection [27] were proposed. Physical methods for transdermal agent delivery have two advantages over formulations and chemical enhancers; (a) interaction between enhancer and the agents being delivered is absent; and

[1] The article is published in the original.

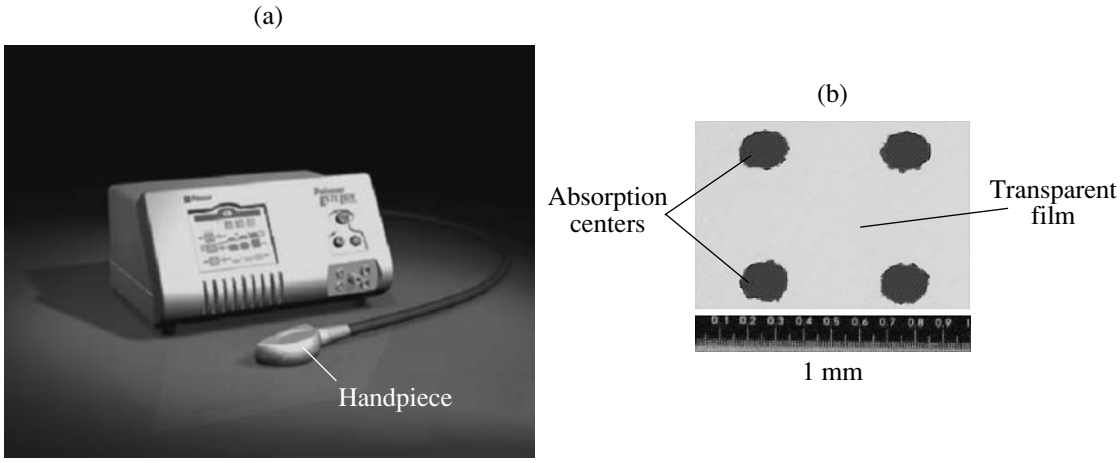


**Fig. 1.** Flash-lamp appliqué system: (a) flash lamp (EsteLux system, Palomar Medical Products Inc., Burlington, Massachusetts) with a handpiece, and (b) a specially designed applique on the basis of a transparent film with absorbing centers.

(b) they reduce the risk of additional skin irritation. However, some methods, such as stripping and laser ablation of skin surface, can be related with the damage or ablation of large areas of *stratum corneum*. Iontophoresis results in a reduction of the resistance of the skin to diffusion of ions but as an enhancer of the flux of uncharged molecules it is lesser effective method. Ultrasound and other pressure waves can affect of various skin structures and inner organs due to a large penetration depth that can be undesirable for specific tasks of OCA's delivery. There is therefore a need to develop alternative methods providing skin barrier permeability for OCAs.

Recently, a method of accelerating penetration of the OCAs due to enhancing epidermal permeability via creating a lattice of micro-zones (islets) of limited photothermal damage or lattice of islets of damage (LID) in the *stratum corneum* (SC) was proposed [28, 29], LID are created as a result of absorption of a sufficient amount of optical energy by the lattice of micro-zones. The absorption leads to temperature elevation in the localized zones of interaction. Since zones of interaction (microdots) contact the skin surface, some of the thermal energy will be conducted to the SC [28]. As the damage of the SC is not a damage of viable tissue, long-term effect of such damage is only the transient deterioration of skin barrier function. That leads to the local increase of OCA's penetration [28]. The lattice of optical islets can be formed using a variety of energy sources and delivery optics, including application of lenslet arrays, phase masks, and matrices of exogenous chromophores [28, 29].

The goal of the paper is the research of skin immersion clearing for the improvement of absorption of laser radiation by tattoo pigments, which are found in skin at some depth, for their destruction by selective laser thermolysis, and for the tattoo visualization, and investigation of effectiveness of the LID-method for enhancement of OCAs penetration rate through SC.

## 2. MATERIALS AND METHODS

### *2.1. Tissue Samples*

Experiments were performed with in vitro full-thickness human skin samples obtained post-surgically from middle-aged humans. The samples were stored in saline from 20 to 24 h after excision. The samples were studied after adipose layer removing. Before the experiments thickness of the samples was measured by micrometer with accuracy of the measurements ±50 μm. Mean thickness of the skin samples was $1.70 \pm 0.25$ mm.

### *2.2. Immersion Agent*

As immersion agent aqueous 88%-glycerol solution (Ecolab, Russia) was used. Refractive index of the glycerol solution measured by Abbe refractometer (IRF-454B2M, Russia) was 1.45.

### *2.3. Flashlamp-Appliqué System*

For the perforation of skin *stratum corneum* a light/appliqué system including a flash-lamp (EsteLux System, Palomar Medical Products Inc., USA) (Fig. 1a) and specially designed appliqué (Fig. 1b) was used. The Palomar EsteLux System was designed to deliver light pulses (10–100 ms) of broadband incoherent light to a predetermined target site. Output wavelengths range was from 400 to 1400 nm. The applique was a transparent plastic film with a pattern of absorbing centers (dots). Diameter of the dots was ~150 μm; distance between the dots was ~500 μm. Regime of the irradiation was 2 pulses with fluence 27 J/cm$^2$. The dots were made out of inert and biocompatible carbon powder,

**Table 1.** The parameters of skin layers used in the simulation [28]

| Skin layers | Thickness, μm | Refractive index | Water content, % | Blood content, % | Scattering coefficient of a bloodless tissue at 577 nm ($cm^{-1}$) | Mean vessel diameter, μm |
|---|---|---|---|---|---|---|
| Epidermis (including stratum corneum) | 100 | 1.45 | 60 | 0 | 300 | – |
| Basal membrane | 15 | 1.4 | 60 | 0 | 300 | – |
| Dermis with upper vessel plexus | 200 | 1.38 | 75 | 1.7 | 120 | 6 |
| Reticular dermis | 1500 | 1.35 | 75 | 1.4 | 120 | 15 |
| Dermis with lower vessel plexus | 200 | 1.38 | 75 | 1.7 | 120 | 6 |
| Subcutaneous adipose layer | 3000 | 1.44 | 5 | 0 | 130 | – |

ensuring high absorption of light energy. The dots absorbed the light energy, which resulted in rapid temperature elevation. The appliqué closely contacted the skin surface to avoid energy dissipation and localize light absorption and, thus, the thermal damage, within the thin surface layer.

The size of the island damage mask was $10 \times 20$ mm and corresponded to a handpiece window of the flashlamp system. As a result of thermal action LID with diameters of craters $200 \pm 20$ μm and depth $25 \pm 5$ μm arose on the surface of the skin samples. To remove products of the thermal action from the craters alcohol (aqueous 40%-ethanol solution) compress was applied on the skin surface for 15 min.

### *2.4. Tattoo Preparation*

Tattoo was prepared on the human skin samples in vitro with the size about $5 \times 5$ $cm^2$. Four crosses were made on the side of dermis. The size of the crosses was $1 \times 1$ $cm^2$. The epidermis of the skin sample was treated in the areas related to the crosses by the different ways. The first area was perforated by flashlamp-appliqué system (2 pulses with fluence 27 J/$cm^2$ and 20 ms pulse duration) and thereafter treated by glycerol solution, the second one was treated by glycerol solution with only flash-lamp pulses without appliqué, the third area—only glycerol action, and the fourth area was saved without any treatment. In the experiments the skin samples were fixed on a cuvette with glycerol solution so that the immersion agent interacted with corresponding areas of skin epidermis only. From the site of dermis the samples were covered by polyethylene film to avoid dehydration of skin.

Black ink was used for the tattooing. Absorption coefficients of the diluted ink solution with concentration 0.25 μL/mL (0.025%, v/v) were measured using spectrophotometer with integrating sphere Lambda 950, Perkin Elmer, USA at wavelengths 470, 532, 650, 694, 850, and 1064 nm and recalculated to 100% concentration. The absorption coefficients are 11770, 10776, 8673, 7872, 6150, and 5253 $cm^{-1}$, respectively.

Nikon Coolpix 995 digital camera (Nikon, Japan) was used to take pictures of the skin samples before treatment, 24 h after treatment, and 2, 3, 4, 5 and 6 days post treatment.

### *2.5. Monte Carlo Simulation*

The efficiency of delivery of laser radiation to the areas of tattoo pigment localization was estimated using Monte Carlo (MC) simulations of variations in the optical properties of skin.

Skin is a complex heterogeneous structure consisting of three main layers: epidermis (100 μm thick), dermis (1–2 mm thick), and subcutaneous adipose tissue (from 1 to 6 mm thick) [24]. The optical properties of these layers are characterized by absorption $\mu_a$ and scattering $\mu_s$ coefficients, and anisotropy factor $g$, which is the average cosine of scattering angle. Distribution of blood, water, melanin and other chromophores in skin produces variations in the optical properties of each layer. These variations allow subdividing each skin layer into sublayers. Epidermis is subdivided into two sublayers: *stratum corneum* (~20 μm thick), which is composed of dry keratinized cellular remains, and *living epidermis* (~100 μm thick) containing a main skin pigment—melanin. Dermis is a main skin layer comprising blood; in turn, it can be subdivided into three main sublayers: *dermis with upper blood net plexus* (200 μm thick), *reticular dermis* (~1.5 mm thick) and *dermis with deep blood net plexus* (200 μm thick). Between epidermis and dermis, a 15-μm-thick basal membrane is located [24, 28].

Absorption properties of skin are mainly determined by the absorption of the following components: melanin, water, and blood hemoglobin. Scattering is determined by the fibrous structure of the tissue, i.e., by scattering on collagen fibrils of dermis and components of mitochondria and nuclei of epidermal cells. In accordance with the optical and the structural-morphological properties of skin, the six-layer skin model is used; its main parameters are presented in Table 1.

In visible and NIR spectral ranges, absorption in each layer is determined by the absorption of three

basis skin chromophores: blood, melanin and water. The absorption coefficient of each layer is defined as:

$$\mu_{ak} = B_k C_k \mu_a^{\text{bl}}(\lambda) + (1 - B_k - W_k)\mu_a^{\text{bg}} + M_k \mu_a^{\text{mel}}(\lambda) + W_k \mu_a^{\text{w}}(\lambda), \quad (1)$$

where $k = 1, \ldots, 6$ is a layer number, $B_k$ and $W_k$ are the volume fractions of blood and water in the each layer; for the melanin containing layers (epidermis and basal membrane) $M_k = 1$, for the other skin layers $M_k = 0$; $\mu_a^{\text{bl}}$, $\mu_a^{\text{mel}}$, $\mu_a^{\text{w}}$, and $\mu_a^{\text{bg}}$ are the absorption coefficients of blood, melanin, water and background matter (collagen) of tissue, respectively (in the framework of the model $\mu_a^{\text{bg}}$ is assumed to be wavelength independent and equal to 0.15 cm$^{-1}$ [28]); $C_k$ is a dimensionless correction factor. The correction factor is a number from 0 to 1 taking into account the fact that blood is localized in vessels rather than distributed homogeneously in the skin dermis. If the blood vessel diameter is large enough, and light does not penetrate to the inner part of the vessel, then hemoglobin of the interior part has not to be taken into account as an absorber; and in this case, the correction factor will be considerably smaller than unity. Otherwise, for thin vessels the correction factor is close to a unity. Taking into account that the correction factor depends on the vessel diameter, we used in the model the following empiric expression [30]:

$$C_k = \frac{1}{1 + a(0.5\mu_a^{\text{bl}} d_k^{\text{ves}})^b}, \quad (2)$$

where $d_k^{\text{ves}}$ is the blood vessel diameter in centimeters and $\mu_a^{\text{bl}}$ should be expressed in inverse centimeters. If blood vessels lying parallel to the skin surface are illuminated by a collimated light beam $a = 1.007$ and $b = 1.228$, while for the diffuse illumination of the vessels $a = 1.482$ and $b = 1.151$. The blood optical properties (i.e., anisotropy factor and both absorption and scattering coefficients) were calculated on the base of algorithm described in details in [31]. In the framework of the modeling it was assumed that degree of hemoglobin oxygenation is 0.8 (because the degree hemoglobin oxygenation for arterial blood is 0.9 and that for venous blood is 0.7). The value of blood hematocrit is 0.4. Now the optical properties of water are well investigated; we used the data presented in [32, 33].

The scattering coefficient of skin layers is defined as:

$$\mu_{sk}(\lambda) = B_k C_k \mu_s^{\text{bl}}(\lambda) + (1 - B_k)\mu_{sk}^{\text{bg}}(\lambda). \quad (3)$$

Here,

$$\mu_{sk}^{\text{bg}}(\lambda) = \mu_{sk}^0(577/\lambda)$$

is the scattering coefficient of bloodless tissue [28]; $\mu_{sk}^0$ is the scattering coefficient of bloodless tissue at the wavelength 577 nm (see Table 1); $\lambda$ is expressed in nanometers.

The anisotropy scattering factor is expressed in the following form:

$$g_k(\lambda) = \frac{B_k C_k \mu_s^{\text{bl}}(\lambda) g^{\text{bl}} + (1 - B_k)\mu_{sk}^{\text{bg}}(\lambda) g^{\text{bg}}(\lambda)}{\mu_{sk}(\lambda)}, \quad (4)$$

where

$$g^{\text{bg}}(\lambda) = 0.7645 + 0.2355\left[1 - \exp\left(-\frac{\lambda - 500}{729.1}\right)\right]$$

is the anisotropy scattering factor of bloodless tissue [28]. The melanin absorption coefficient in the model is defined on the base of empiric expression [28]

$$\mu_a^{\text{mel}}(\lambda) = A \exp\left(-\frac{\lambda - 800}{182}\right), \quad (5)$$

where the parameter $A$ is the ratio of the optical density of pigmented skin layer (epidermis and basal membrane) to their thickness. In the model $A = 0.87$ cm$^{-1}$ for epidermis and 13.5 cm$^{-1}$ for basal membrane [28].

The optical clearing of different skin layers was simulated using Mie scattering theory [34], which requires the knowledge of the refractive indices of skin scatterers and surrounding interstitial fluid, and also sizes of the scatterers. Calculations for epidermis and basal membrane have been performed using the model of spherical particles, while for dermis the model of cylindrical particles was used. The choice of spherical scatterers for the describing of epidermal scattering properties is based on the fact that cell mitochondria are the main scatterers for epithelial tissues [35, 36]; and the choice of cylindrical scatterers for the describing of the scattering in dermis is caused by fibrous structure of dermis [36, 37]. Because the particle size distribution and the packing factor of the scatterers are unknown, monodisperse, so-called Mie-equivalent particles were used for the simulation.

The scattering coefficients of upper skin layers was calculated in the form

$$\mu_s(\lambda) = \frac{3}{4}\frac{\varphi}{\pi a_{\text{sph}}^3}\pi a_{\text{sph}}^3 Q_s(a_{\text{sph}}, n_s, n_I)F(\lambda), \quad (6)$$

where $a_{\text{sph}}$ is the radius of spherical scatterers; $Q_s(a_{\text{sph}}, n_s, n_I)$ is the scattering efficiency factor; $F(\lambda)$ is the packing factor of scatterers; $n_s$ is the refractive index of scatterers; $n_I$ is the refractive index of interstitial fluid; $\varphi$ is the volume fraction of scatterers for each layer. For dermal layers the scattering coefficient was calculated as

$$\mu_s(\lambda) = \frac{\varphi}{\pi a_c^2} 2a_c Q_s(a_c, n_s, n_I)F(\lambda), \quad (7)$$

where $a_c$ is the radius of cylindrical scatterers. Both the effective size of scatterers and the packing factor were calculated by the minimization of the target function

$$\mathrm{TF}(a(\lambda), F(\lambda)) = (\mu_s^{\mathrm{mod}} - \mu_s^{\mathrm{Mie}})^2 + (g^{\mathrm{mod}} - g^{\mathrm{Mie}})^2. \quad (8)$$

Here, $\mu_s^{\mathrm{mod}}$ and $g^{\mathrm{mod}}$ correspond to the data calculated according to Eqs. (3) and (4) for each layer; $\mu_s^{\mathrm{Mie}}$ and $g^{\mathrm{Mie}}$ are the scattering coefficient (Eqs. (6), (7)) and the anisotropy factor calculated for each layer on the base of Mie theory. To minimize the target function the Nelder and Mead simplex method described in detail by [38] has been used.

The influence of clearing agent on the skin optical properties was modeled by replacing the interstitial fluid by the clearing agent (aqueous glycerol solution) with the refractive index higher than that of the interstitial fluid. Calculations were performed by assuming that the refractive index of skin interstitial fluid equals to that of water, and the refractive index of aqueous glycerol solution is 1.45. It was assumed that the sizes of effective skin scatterers, the packing factor of the scatterers and the refractive index of the scatterers have not being changed during the optical clearing.

For tattoo modeling, absorbing layer in the form of cross with thickness 50 μm and size 1 × 1 cm was added in skin model. Area of the modeled sample of skin was 3 × 3 cm. Absorption coefficient of the layer is equal to absorption coefficient of ink presented in Section 2.4. Scattering properties of this layer is equal to the scattering properties of reticular dermis. The depth of ink location in the model was chosen as 0.5 or 1.0 mm, because mechanical devices for tattooing provide the standard depth of ink injection from 0.2 to 1.0 mm in dependence on techniques and used equipment [16].

The MC simulation has been performed on the base of the algorithm presented in [39]. The stochastic numerical MC method is widely used to modeling of propagation of optical radiation in complex random highly scattering and absorbing medium such as biological tissue. The MC modeling of photon packet trajectories consists in the sequence of the elementary simulations: photon pathlength generation, scattering and absorption events, reflection or/and refraction on medium boundaries. The initial and final states of the photons are entirely determined by the source and detector geometry.

For the calculation of the photon fraction absorbed in tattoo area the following procedure was used: when a photon trajectory passed through tattoo area, parameter $A_t$ (the photon fraction absorbed in tattoo area) increased on $w\mu_a/(\mu_a + \mu_s)$ at the each act of interaction [39], where w is the current weight of photon packet, and $\mu_a$ and $\mu_s$ are the coefficients of absorption and scattering in the given point, respectively. After the detection of all photon packets the value $A_t$ was summed over all packets and normalized on the total weigh of the packets, which were used for the simulation.

A new propagation direction of the scattered photon packet was determined according to the Henyey–Greenstein scattering phase function:

$$f_{\mathrm{HG}}(\theta) = \frac{1}{4\pi}\frac{1 - g^2}{(1 + g^2 - 2g\cos\theta)^{3/2}},$$

where θ is the polar scattering angle. The distribution over the azimuthal scattering angle was assumed as uniform.

For the simulation of skin images with tattoo $25 \times 10^6$ photon packets was used. Photons normally incident on the skin surface were uniformly distributed over the area 3 × 3 cm. For the detection of backscattered photons this area (3 × 3 cm) was separated on the grid with area of the grid cells of 0.01 mm$^2$. When backscattered photon went out, its weigh was recorded to the array cell, which corresponded to the coordinates of the point of going out, then was summed over all packets. After the finish of the simulation it was normalized on the average weigh of the incident packets upon correspondent area.

The thickness and refractive indices of skin layers used in the MC simulations are presented in Table 1. Absorption coefficients for each wavelength and each layer were calculated in accordance with Eq. (1), and the scattering coefficients and the anisotropy factors of each skin layer without optical clearing were calculated in accordance with Eqs. (3) and (4). At the immersion clearing of skin the both scattering coefficient and anisotropy factor of each skin layer were calculated in accordance with Eqs. (6), (7) and Mie theory [34].

## 3. RESULTS AND DISCUSSION

Figure 2 shows human skin samples with black tattoo before and after the treatment with the aqueous glycerol solution for 24 h and 6 days, respectively. The stratum corneum of the skin samples was previous perforated only on the area no. 1. It is well seen that in the initial moment (Fig. 2a) tattoo were visualized significantly worse than after treatment and immersion (Figs. 2b, 2c). In the figure it is well seen that maximal clearing effect was reached for the area no. 1, which is treated by glycerol after two flash-lamp pulses and appliqué. Only a slight clearing effect was observed at the other sites treated without appliqué (no. 2), with glycerol only (no. 3), and without any treatment (no. 4). Thus, the use of LID allows for more effective transepidermal delivery of optical clearing agent and increasing tattoo image contrast.

Monte Carlo simulations of skin images with black tattoo localized in reticular dermis of skin at the depth of 0.5 and 1.0 mm are presented in Figs. 3a–8a, 3b–8b and Figs. 3c–8c, 3d–8d, respectively. The images were simulated using optical properties of skin calculated at

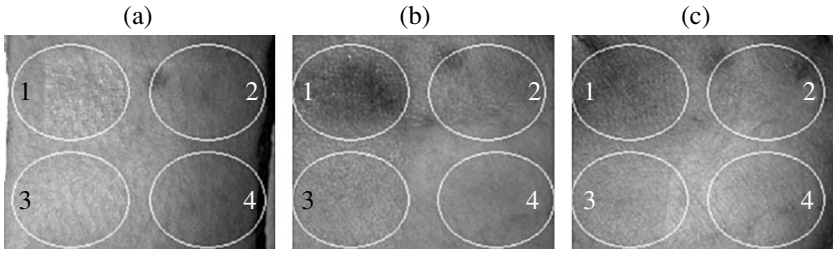


**Fig. 2.** Photographs of the skin sample with tattoo under action of 88%-glycerol solution in vitro 1—glycerol action after two flash-lamp pulses with fluence 27 J/cm$^2$, 20 ms pulse duration and appliqué; 2—glycerol action with only the flash-lamp pulses without appliqué; 3—only glycerol action; 4—without any influence: (a) before glycerol applying; (b) after 24 h of glycerol action and (c) after 6 days of glycerol action.

$\lambda$ = 470 nm (Fig. 3), 532 nm (Fig. 4), 650 nm (Fig. 5), 694 nm (Fig. 6), 850 nm (Fig. 7), and 1064 nm (Fig. 8). Choice of the wavelengths connected with laser wavelengths, which usually used for tattoo removal. For this images letters (a) and (c) correspond to skin without clearing and letters (b) and (d) correspond to case when skin layers lying above the tattoo are immersed by the clearing agent (glycerol solution) administered topically. Earlier we have demonstrated [40] that this method (topical administration) of clearing agent delivery is more preferable for tattoo visualization in comparison with intradermal injection, because provides higher tattoo contrast. The simulation of photon transport in skin has shown that the immersion of layer lying under tattoo decreases the number of photons absorbed in the given area [40]. It is explained by the fact that the photons, which have passed through upper skin layers and the layer with the tattoo ink to the weakly scattering area propagate through this area without the changing their propagation direction and are absorbed in deeper skin layers. Thus, they cannot make the contribution to the photon fraction absorbed in tattoo area. At the same time, when only upper layers lying over the staining layer are cleared, a significant number of photons propagate through the upper layers almost without scattering and are absorbed in the tattoo area. In this case, pho-

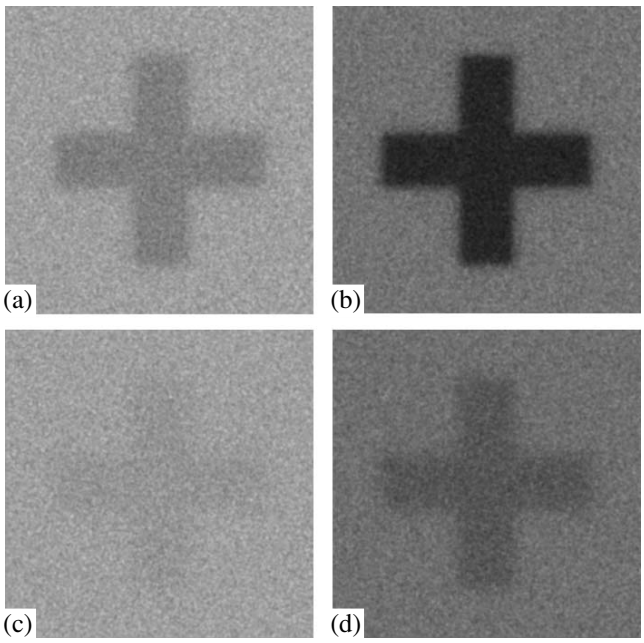


**Fig. 3.** Result of MC simulation of skin tattoo images at wavelength 470 nm, the depth of the tattoo is 0.5 (a, b) and 1.0 (c, d) mm, the size of the tattoo is 1 × 1 cm, the area of the simulated skin samples is 1 × 1 cm: skin without clearing (a, c); skin layers lying above the tattoo are immersed by the agent administering topically (b, d).

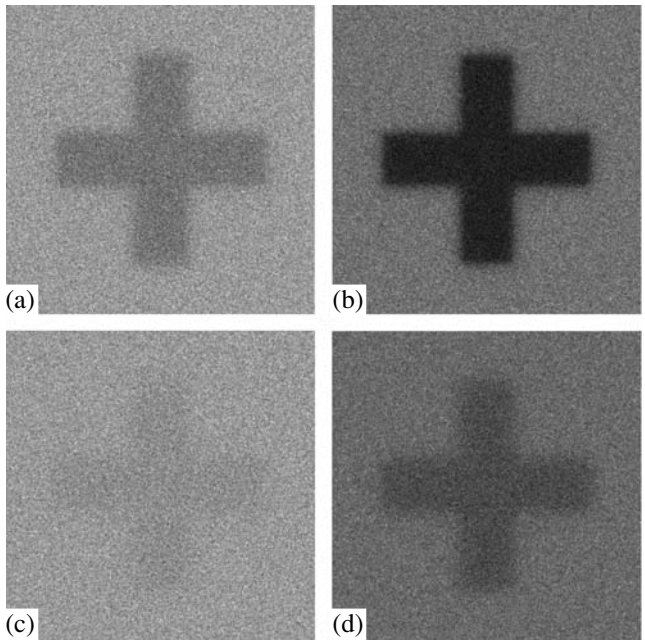


**Fig. 4.** Result of MC simulation of skin tattoo images at wavelength 532 nm, the depth of the tattoo is 0.5 (a, b) and 1.0 (c, d) mm, the size of the tattoo is 1 × 1 cm, the area of the simulated skin samples is 1 × 1 cm: skin without clearing (a, c); skin layers lying above the tattoo are immersed by the agent administering topically (b, d).

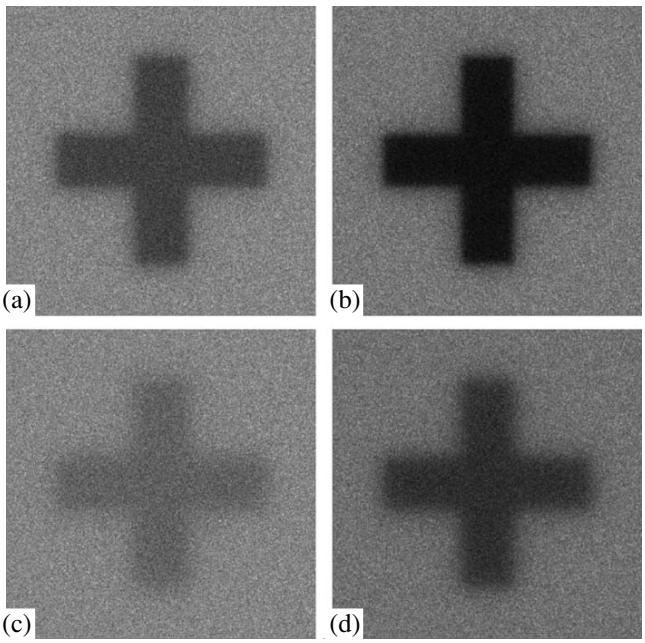


**Fig. 5.** Result of MC simulation of skin tattoo images at wavelength 650 nm, the depth of the tattoo is 0.5 (a, b) and 1.0 (c, d) mm, the size of the tattoo is $1 \times 1$ cm, the area of the simulated skin samples is $1 \times 1$ cm: skin without clearing (a, c); skin layers lying above the tattoo are immersed by the agent administering topically (b, d).

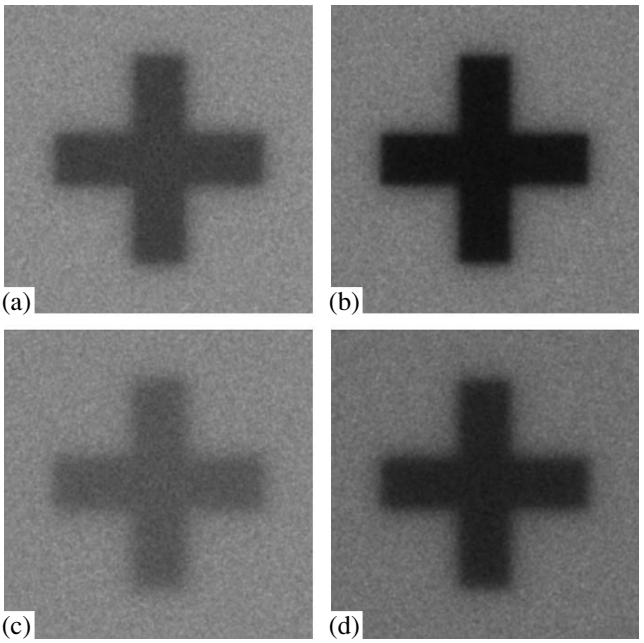


**Fig. 6.** Result of MC simulation of skin tattoo images at wavelength 694 nm, the depth of the tattoo is 0.5 (a, b) and 1.0 (c, d) mm, the size of the tattoo is $1 \times 1$ cm, the area of the simulated skin samples is $1 \times 1$ cm: skin without clearing (a, c); skin layers lying above the tattoo are immersed by the agent administering topically (b, d).

tons which have passed through the absorbing layer to the area under the tattoo can after the scattering in lower layers return into the staining layer and be absorbed there. Thus, the clearing of upper skin layers allows significantly reduces the laser power used for thermolysis by increasing light absorption in tattoo. However, it is important to know how the optical clearing can improve the tattoo visualization and decrease of power of radiation used for tattoo removal by laser thermolysis in dependence on choice of wavelength of irradiation.

The tattoo borders in the Figs. 3–8 look rather blurred (it is especially seen in the images of deep tattoos (~1 mm) (Figs. 3c–8c), due to high light scattering by upper tissue layers. The optical clearing of the layers significantly enhances the image contrast, which improves the tattoo localization and visualization. The image contrast was estimated by the expression $K = (R_1 - R_2)/(R_1 + R_2)$, where $R_1$ and $R_2$ are the skin reflectance outside the tattoo area and inside it, respectively, and result of the calculations was summarized and presented in Table 2.

**Table 2.** Result of MC simulation of contrast of tattoo images

| | Tattoo depth is 0.5 mm | | | Tattoo depth is 1.0 mm | | |
|---|---|---|---|---|---|---|
| Wavelength, nm | upper skin layers are immersed ($K^{\text{skin}}_{\text{immersed}}$) | skin without clearing ($K^{\text{skin without}}_{\text{clearing}}$) | $\frac{K^{\text{skin}}_{\text{immersed}}}{K^{\text{skin without}}_{\text{clearing}}}$ | upper skin layers are immersed ($K^{\text{skin}}_{\text{immersed}}$) | skin without clearing ($K^{\text{skin without}}_{\text{clearing}}$) | $\frac{K^{\text{skin}}_{\text{immersed}}}{K^{\text{skin without}}_{\text{clearing}}}$ |
| 470 | 0.261 | 0.075 | 3.480 | 0.070 | 0.022 | 3.182 |
| 532 | 0.316 | 0.099 | 3.192 | 0.100 | 0.028 | 3.571 |
| 650 | 0.526 | 0.257 | 2.047 | 0.284 | 0.113 | 2.513 |
| 694 | 0.552 | 0.288 | 1.917 | 0.382 | 0.166 | 2.301 |
| 850 | 0.584 | 0.362 | 1.613 | 0.380 | 0.172 | 2.209 |
| 1064 | 0.545 | 0.378 | 1.442 | 0.371 | 0.181 | 2.050 |

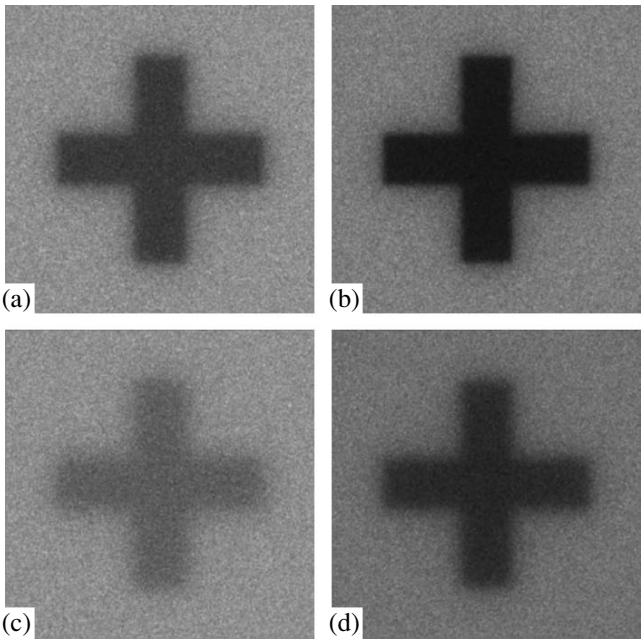


**Fig. 7.** Result of MC simulation of skin tattoo images at wavelength 850 nm, the depth of the tattoo is 0.5 (a, b) and 1.0 (c, d) mm, the size of the tattoo is $1 \times 1$ cm, the area of the simulated skin samples is $1 \times 1$ cm: skin without clearing (a, c); skin layers lying above the tattoo are immersed by the agent administering topically (b, d).

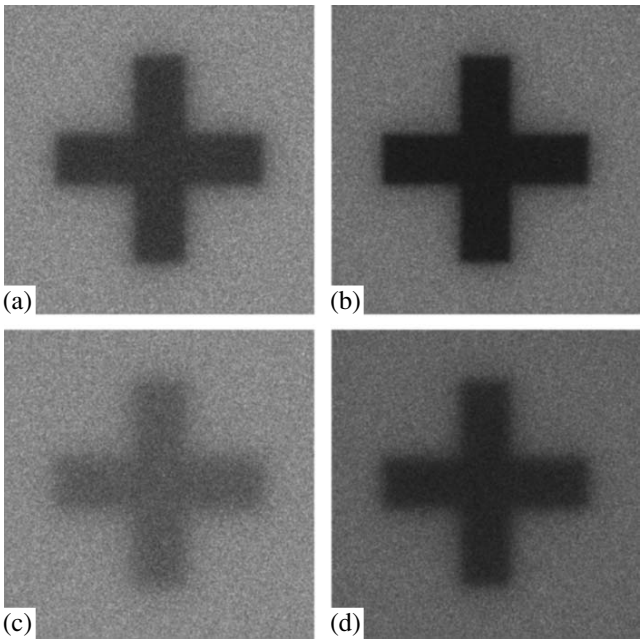


**Fig. 8.** Result of MC simulation of skin tattoo images at wavelength 1064 nm, the depth of the tattoo is 0.5 (a, b) and 1.0 (c, d) mm, the size of the tattoo is $1 \times 1$ cm, the area of the simulated skin samples is $1 \times 1$ cm: skin without clearing (a, c); skin layers lying above the tattoo are immersed by the agent administering topically (b, d).

In Fig. 3 results of MC simulation of skin tattoo located at the depth of 0.5 (Figs. 3a, 3b) and 1.0 mm (Figs. 3c, 3d) at illumination of the skin by light with wavelength 470 nm are presented. It is seen that in initial time tattoo, which located at the depth of 0.5 mm (Fig. 3a) poorly seen and tattoo, which located at the depth of 1.0 mm (Fig. 3c) is practically not observed. However, after optical clearing of skin layers lying above the tattoo we can observe the tattoos, especially when the tattoo located at the depth of 0.5 mm (Fig. 3b). Before clearing the image contrast of tattoo located at the depth of 0.5 mm against the background of intact skin $K = 0.075$. After the skin optical clearing the contrast is significantly increased ($K = 0.261$). For tattoo located at the depth of 1.0 mm (Figs. 3c, 3d) we have $K = 0.022$ for intact skin and $K = 0.07$ after the skin clearing.

Similar result has been obtained for illumination of skin by light with wavelength 532 nm (Fig. 4). In this case the image contrast for tattoo located at the depth of 0.5 mm is 0.099 for skin without clearing and $K = 0.316$ after clearing the upper layers of the skin. For tattoo located at the depth of 1.0 mm (Figs. 4c, 4d) we have $K = 0.028$ for intact skin and $K = 0.1$ after the skin clearing.

At use of red light for the skin illumination (see Figs. 5 and 6) the situation is appreciably change. In this case we can observe tattoo even the deeply (1.0 mm (Figs. 5c and 6c)) embedded in intact skin. Analysis of the Figs. 5a, 5b shows that contrast of tattoo is increased from 0.257 to 0.526 for tattoo located at the depth of 0.5 mm (at illumination wavelength is 650 mm). For tattoo located at the depth of 1.0 mm (Figs. 5c, 5d) we have the contrast increasing from 0.113 to 0.284. In case when we use light with wavelength 694 nm for skin illumination (Fig. 6) we obtained the contrast increasing from 0.166 to 0.382 for deeply embedded tattoo (Figs. 6c, 6d) and from 0.288 to 0.552 for tattoo located at the depth of 0.5 mm (Figs. 6a, 6b). In near-infrared spectral range for wavelengths of the skin illumination 850 (Fig. 7) and 1064 nm (Fig. 8) the similar result has been obtained. For tattoo located at the depth of 0.5 mm (Figs. 7a, 7b) we have the contrast increasing from 0.362 to 0.584, and for tattoo located at the depth of 1.0 mm (Figs. 7c, 7d) we have the increase of the contrast from 0.172 to 0.380. For illumination of the skin by light with wavelength 1064 nm (Fig. 8) we observe the increase of the contrast from 0.378 to 0.545 for tattoo located at the depth of 0.5 mm (Figs. 8a, 8b) and from 0.181 to 0.371 for tattoo located at the depth of 1.0 mm (Figs. 8c, 8d).

These results are summarized and presented in Table 2. From the table it is seen that contrast of the tattoo images increases with increasing of wavelength of illuminating radiation especially in the visible spectral range. At the same time, ratio of the contrast images of tattoo embedded in immersed skin to the contrast

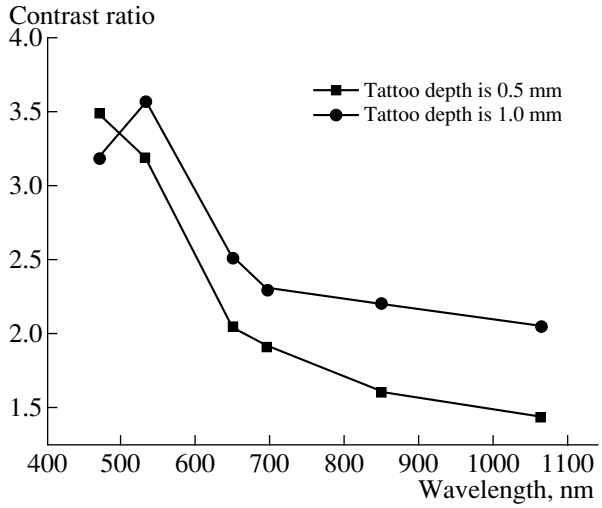


**Fig. 9.** The contrast ratio of the tattoo images: $K^{\text{skin}}_{\text{immersed}}/K^{\text{skin without}}_{\text{clearing}}$.

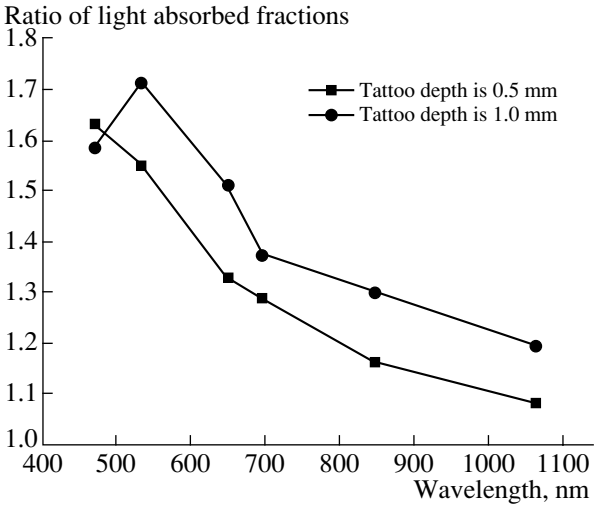


**Fig. 10.** The ratio of light absorbed fractions in tattoo area with and without skin optical clearing: $A^{\text{skin}}_{\text{immersed}}/A^{\text{skin without}}_{\text{clearing}}$.

images of tattoo embedded in native skin decreases with wavelength increasing. The ratio decreases from 3.48 ($\lambda$ = 470 nm) to 1.442 ($\lambda$ = 1064 nm) for tattoo located at the depth of 0.5 mm; and from 3.182 ($\lambda$ = 470 nm) to 2.05 ($\lambda$ = 1064 nm) for tattoo located at the depth of 1.0 mm (see Fig. 9). Thus, from analysis of the table we can conclude that the technique of optical clearing can be maximally applied to improve of tattoo visualization at use for the purposes of short-wavelength lasers or other light sources.

Fraction of photons absorbed in the tattoo area has been calculated in accordance with algorithm described in Section 2.5 and the result is presented in Table 3. From the table we have seen that the fraction increases with the increase of wavelength similar to the contrast, and ratio of the light fraction absorbed in tattoo embedded in immersed skin to the fraction for tattoo embedded in native skin decreases with wavelength increasing (see Fig. 10). The ratio decreases from 1.588 ($\lambda$ = 470 nm) to 1.197 ($\lambda$ = 1064 nm) for tattoo located at the depth of 1.0 mm and from 1.633 ($\lambda$ = 470 nm) to 1.082 (1064 nm) for tattoo located at the depth of 0.5 mm. That is connected with decreasing of skin scattering with increasing of wavelength; so more photons propagate to absorbing layer and are absorbed within tattoo, i.e. the effect is similar to the clearing effect.

For estimation of effectiveness of the optical clearing for reducing of laser power density applied in photothermolysis, we have used literature data. In particular, the density of irradiation energy of a frequency-doubled Nd:YAG laser ($\lambda$ = 532 nm) used for tattoo removal is 2–4 [41], 3 [6], and 2.6 J/cm$^2$ [42]. For a ruby laser ($\lambda$ = 694 nm) the energy density is 3.5 [4] or 4–7 J/cm$^2$ [41]. The energy density of a Q-switched alexandrite laser ($\lambda$ = 755 nm) is 5 [6, 8], 7.16 [11], and 10–16 J/cm$^2$ [42]. For Q-switched Nd:YAG laser ($\lambda$ =

**Table 3.** Result of MC simulation of light absorbed fraction in tattoo area

| Wavelength, nm | Tattoo depth is 0.5 mm | | | Tattoo depth is 1.0 mm | | |
|---|---|---|---|---|---|---|
| | upper skin layers are immersed ($A^{\text{skin}}_{\text{immersed}}$) | skin without clearing ($A^{\text{skin without}}_{\text{clearing}}$) | $\frac{A^{\text{skin}}_{\text{immersed}}}{A^{\text{skin without}}_{\text{clearing}}}$ | upper skin layers are immersed ($A^{\text{skin}}_{\text{immersed}}$) | skin without clearing ($A^{\text{skin without}}_{\text{clearing}}$) | $\frac{A^{\text{skin}}_{\text{immersed}}}{A^{\text{skin without}}_{\text{clearing}}}$ |
| 470 | 0.049 | 0.030 | 1.633 | 0.027 | 0.017 | 1.588 |
| 532 | 0.059 | 0.038 | 1.553 | 0.036 | 0.021 | 1.714 |
| 650 | 0.081 | 0.061 | 1.328 | 0.068 | 0.045 | 1.511 |
| 694 | 0.085 | 0.066 | 1.288 | 0.077 | 0.056 | 1.375 |
| 850 | 0.093 | 0.080 | 1.163 | 0.086 | 0.066 | 1.303 |
| 1064 | 0.092 | 0.085 | 1.082 | 0.085 | 0.071 | 1.197 |

1064 nm) the energy density is 4–8 [41] and 5 J/cm$^2$ [42]. From the data presented in Table 3 there is following that in the area of tattoo localized at the depth of 0.5 mm the light absorbed fraction is 0.038 for $\lambda$ = 532 nm, 0.066 for $\lambda$ = 694 nm, 0.085 for $\lambda$ = 1064 nm, and the light absorbed fraction can be estimated as 0.07 for $\lambda$ = 755 nm, which correspond to the density of energy in tattoo area: $0.11 \pm 0.03$ J/cm$^2$ for $\lambda$ = 532 nm, $0.32 \pm 0.12$ J/cm$^2$ for $\lambda$ = 694 nm, $0.67 \pm 0.33$ J/cm$^2$ for $\lambda$ = 755 nm, and $0.48 \pm 0.18$ J/cm$^2$ for $\lambda$ = 1064 nm. In the case of skin clearing the absorbed photon fraction increases up to 0.059 for $\lambda$ = 532 nm, 0.085 for $\lambda$ = 694 nm, 0.092 for $\lambda$ = 1064 nm, and 0.09 for $\lambda$ = 755 nm (estimated), which correspond to the density of energy in tattoo area: $0.17 \pm 0.05$ J/cm$^2$ for $\lambda$ = 532 nm, $0.41 \pm 0.16$ J/cm$^2$ for $\lambda$ = 694 nm, $0.86 \pm 0.43$ J/cm$^2$ for $\lambda$ = 755 nm, and $0.52 \pm 0.19$ J/cm$^2$ for $\lambda$ = 1064 nm. In the area of tattoo localized at the depth of 1.0 mm the light absorbed fraction is 0.021 for $\lambda$ = 532 nm, 0.056 for $\lambda$ = 694 nm, 0.06 for $\lambda$ = 755 nm (estimated), 0.071 for $\lambda$ = 1064 nm, which correspond to the density of energy in tattoo area: $0.06 \pm 0.02$ J/cm$^2$ for $\lambda$ = 532 nm, $0.27 \pm 0.11$ J/cm$^2$ for $\lambda$ = 694 nm, $0.57 \pm 0.29$ J/cm$^2$ for $\lambda$ = 755 nm, and $0.40 \pm 0.15$ J/cm$^2$ for $\lambda$ = 1064 nm. In the case of skin clearing the absorbed photon fraction increases up to 0.036 for $\lambda$ = 532 nm, 0.077 for $\lambda$ = 694 nm, 0.08 for $\lambda$ = 755 nm (estimated), 0.085 for $\lambda$ = 1064 nm, which correspond to the density of energy in tattoo area: $0.10 \pm 0.03$ J/cm$^2$ for $\lambda$ = 532 nm, $0.37 \pm 0.15$ J/cm$^2$ for $\lambda$ = 694 nm, $0.76 \pm 0.38$ J/cm$^2$ for $\lambda$ = 755 nm, and $0.48 \pm 0.18$ J/cm$^2$ for $\lambda$ = 1064 nm. Thus, to achieve the same result, which can be obtained without skin optical clearing, the density of laser energy can be reduced on 50–60% in dependence on the tattoo localization depth in blue-green spectral range, on 30–40% in red spectral range, and 10–20% in near-infrared spectral range.

## 4. CONCLUSIONS

In the paper the result of immersion optical clearing of upper skin layers at the administering of ink into dermis is presented. The possibility improvement of selective laser thermolysis on the wavelengths 470, 532, 650, 694, 850, and 1064 nm, which are the most often used in tattoo laser removal was analyzed. From the data obtained with MC simulation skin images with tattoo located at different depths in dermis were made. It was shown that at the clearing of upper skin layers the photon fraction absorbed in tattoo areas at the depths of 0.5 or 1.0 mm increases, that allows significant decreasing of the power of laser radiation used at thermolysis. It has been concluded that the technique of optical clearing can be maximally applied to improve of both tattoo visualization and removal at use for the purposes of short-wavelength lasers or other light sources.

## ACKNOWLEDGMENTS

The study was supported by Palomar Medical Technologies Inc. (Burlington, USA), and grants of the Scientific Leading School (no. 208.2008.2) and RFBR (project no. 06-02-16740).

## REFERENCES

1. R. W. B. Scutt, Br. J. Plast. Surg. **25**, 189 (1972).
2. R. Reid and S. Muller, Plast. Reconstr. Surg. **65**, 717 (1980).
3. D. B. Apfelberg, M. R. Maser, H. Lash, D. N. White, and J. T. Flores, Ann. Plast. Surg. **14**, 6 (1985).
4. M. Huzaira and R. Anderson, Lasers Surg. Med. **31**, 121 (2002).
5. V. J. Levine and R. G. Geronemus, Cutis **55**, 291 (1995).
6. R. J. McNichols, M. A. Fox, A. Gowda, S. Tuya, B. Bell, and M. Motamedi, Lasers Surg. Med. **36**, 289 (2005).
7. S. L. Kilmer, and R. R. Anderson, J. Dermatol. Surg. Oncol. **19**, 330 (1993).
8. R. E. Fitzpatrick and J. R. Lupton, Lasers Surg. Med. **27**, 358 (2000).
9. M. L. Leuenberger, M. W. Mullas, T. R. Hata, M. P. Goldman, R. E. Fitzpatrick, and J. M. Grevelink, Dermatol. Surg. **25**, 10 (1999).
10. T. S. Alster, J. Am. Acad. Dermatol. **33**, 69 (1995).
11. G. A. Moreno-Arias, M. Casals-Andreu, and A. Camps-Fresneda, Lasers Surg. Med. **25**, 445 (1999).
12. R. Mann and G. Klingmuller, Arch. Dermatol. Res. **271**, 367 (1981).
13. J. E. Fergusson, S. M. Andrew, C. J. Jones, and P. J. August, Br. J. Dermatol. **137**, 405 (1997).
14. A. L. Timko, C. H. Miller, F. B. Johnson, and E. V. Ross, Arch. Dermatol. **137**, 143 (2001).
15. S. E. Dozier, D. G. Diven, D. Jones, M. Brysk, R. L. Sanchez, and M. Motamedi, Dermatol. Surg. **21**, 237 (1995).
16. B. D. Zelickson, D. A. Mehregan, A. A. Zarrin, C. Coles, P. Hartwig, S. Olson, and J. Leaf-Davis, Lasers Surg. Med. **15**, 364 (1994).
17. V. V. Tuchin, *Optical Clearing of Tissues and Blood* (SPIE Press, Bellingham, WA, 2005), vol. PM 154.
18. V. V. Tuchin, Laser Phys. **15**, 1109 (2005).
19. J. Lademann, A. Rudolph, U. Jacobi, H.-J. Weigmann, H. Schaefer, W. Sterry, and M. Meinke, J. Biomed. Opt. **9**, 1358 (2004).
20. J.-Y. Fang, W.-R. Lee, S.-C. Shen, Y.-P. Fang, and C.-H. Hu, Br. J. Dermatol. **151**, 132 (2004).
21. J. S. Nelson, J. L. McCullough, T. C. Glenn, W. H. Wright, L. H. L. Liaw, and S. J. Jacques, J. Invest. Dermatol. **97**, 874 (1991).
22. O. Stumpp, A. J. Welch, and J. Neev, Lasers Surg. Med. **37**, 278 (2005).
23. H. E. Bodde, P. E. H. Roemele, and W. M. Star, Photochem. and Photobiol. **75**, 418 (2002).
24. H. Schaefer and T. E. Redelmeier, *Skin Barier: Principles of Percutaneous Absorption* (Karger, Basel, 1996).

25. I. V. Larina, B. M. Evers, T. V. Ashitkov, C. Bartels, K. V. Larin, and R. O. Esenaliev, Technol. Cancer Res. Treatment **4**, 217 (2005).
26. S. Lee, D. J. McAuliffe, N. Kollias, T. J. Flotte, and A. G. Doukas, Laser Surg. Med. **31**, 207 (2002).
27. O. Stumpp and A. J. Welch, Proc. SPIE **4949**, 44 (2003).
28. G. Altshuler, M. Smirnov, and I. Yaroslavsky, J. Phys. D: Appl. Phys. **38**, 2732 (2005).
29. V. V. Tuchin, G. B. Altshuler, A. A. Gavrilova, A. B. Pravdin, D. Tabatadze, J. Childs, and l. V. Yaroslavsky, Lasers Surg. Med. **38**, 824 (2006).
30. A. N. Bashkatov, V. V. Tuchin, E. A. Genina, M. M. Stolnitz, D. M. Zhestkov, G. B. Altshuler, and I. V. Yaroslavsky, Proc. SPIE **6436**, 64360Z (2007).
31. A. N. Bashkatov, D. M. Zhestkov, É. A. Genina, and V. V. Tuchin, Opt. Spectrosc. **98**, 695 (2005).
32. G. Hale and M. R. Querry, Appl. Opt. **12**, 555 (1973).
33. R. C. Smith and K. S. Baker, Appl. Opt. **20**, 177 (1981).
34. C. F. Bohren and D. R. Huffman, *Absorption and Scattering of Light by Small Particles* (Wiley, New York, 1983).
35. J. R. Mourant, J. P. Freyer, A. H. Hielscher, A. A. Eick, D. Shen, and T. M. Johnson, Appl. Opt. **37**, 3586 (1998).
36. V. V. Tuchin, *Tissue Optics: Light Scattering and Instruments for Medical Diagnostics* (SPIE Press, Bellingham, WA, 2007), vol. PM 166.
37. I. S. Saidi, S. L. Jacques, and F. K. Tittel, Appl. Opt. **34**, 7410 (1995).
38. B. Bunday, *Basis Optimization Methods* (Edward Arnold, London, 1984).
39. L. Wang, S. L. Jacques, and L. Zheng, Comput. Methods Programs Biomed. **47**, 131 (1995).
40. E. A. Genina, A. N. Bashkatov, V. V. Tuchin, G. B. Altshuler, and I. V. Yaroslavski, Quantum Electron. **38**, 580 (2008).
41. E. V. Ross, S. Yashar, N. Michaud, R. Fitzpatrick, R. Geronemus, W. D. Tope, and R. R. Anderson, Arch. Dermatol. **137**, 33 (2001).
42. B. M. Prinz, S. R. Vavricka, P. Graf, G. Burg, and R. Dummer, Br. J. Dermatol. **150**, 245 (2004).